On the numerical assessment of flow losses and secondary flows in Pelton turbine manifolds

On the numerical assessment of flow losses and secondary flows in Pelton turbine manifolds

F J J Hahn, B Semlitsch and C Bauer

Institute of Energy Systems and Thermodynamics, Research Unit of Fluid Flow Machinery, TU Wien, Vienna, Austria

E-mail: franz.hahn@tuwien.ac.at

Abstract. Different methods combining analytical guidelines, numerical simulations, and the manufacturer's experience are employed to design and optimise the distributor manifold of a Pelton turbine. All these methods have in common to assume undisturbed straight inflow to the manifold, thus neglecting the upstream flow conditions. Our numerical simulations executed with the open-source code OpenFOAM v2012 show that the insufficient consideration of the upstream flow situation may lead to inaccurate predictions of the manifold flow. Five turbulence models were tested in our simulations, and the inflow turbulence intensity was varied from 1% to 10%. The flow quality was assessed by evaluating the head loss coefficient from total pressure drop, the head loss coefficient from the entropy production, the secondary velocity ratio upstream the injectors and the mass flow imbalances in the injectors. The study of turbulence models revealed that the k-ω Shear Stress Transport model predicted the head loss and secondary flows with reasonable accuracy. Also, the computationally less expensive model of Spalart-Allmaras leads to similar results and therefore emerges as an appropriate model for optimisation. The simulations with varying inflow turbulence intensity levels indicate a flow pattern change, if the specified inflow turbulence intensity is less than 4%. Below this value of inflow turbulence intensity, a significant increase of the secondary flow upstream of the injectors was observed.

1. Introduction

Pelton turbines are employed for electricity generation when the water flow rate is small compared to the head. The water is guided through a headrace tunnel and a penstock line from the high altitude reservoir to the turbine. The potential energy is converted into kinetic energy by forming a free jet at the end of the pressure line. Impinging onto the buckets, the water jet impulse rotates the Pelton turbine runner, which transfers the rotational energy over the shaft to the electric generator.

The distributor line (also referred to as distributor pipe or manifold) is the piping segment upstream of the injectors and divides the flow into equal portions to the injectors. The energy losses should not exceed $2-3\%$ of the total water head in this process. Moreover, the secondary flows, induced by flow separation at abrupt bends and branches, disperse and deviate the free jet as was experimentally investigated by Zhang and Casey [1], and Staubli et al. [2]. Thereby, losses are generated at the runner during the jet-bucket interaction causing a reduction of the turbine efficiency as shown by Peron et al. [3] and Santolin et al. [4]. Wide cross-sections and large curvature radii at pipe bifurcations are desired to mitigate flow separation but increase the frictional losses, the weight and hence the cost of the distributor line. Thus, these design criteria have to be balanced.

Computational simulations aid the distributor design process by assessing the energy losses and the jet flow quality [5, 6, 7, 8]. The turbulent, two-phase nature of the flow demands numerical modelling to enable fast performance predictions required to screen numerous operating scenarios and design configurations. While the Volume-of-Fluid method has become standard to replicate the interface between water and air, various turbulence closures have been applied to pipe flow simulations. The $k-\varepsilon$ model [5], the $k-\varepsilon$ RNG model [8], but mostly the $k-\omega$ SST closure model [7, 9, 10] have been employed in literature. Turbulence modelling is necessary for fluid dynamic optimisation since scale resolving methods are computationally too demanding. Thus, assumptions are needed at the inlet to prescribe the state of turbulence with respect to the quantities, turbulent kinetic energy k, turbulent dissipation rate ε, and/or turbulent frequency ω. The typical engineering assumption of undisturbed inflow has been made in literature [11, 8, 7], while the sensitivity of the simulation to such assumptions has not been studied yet.

Numerical flow simulations can predict the implications of imperfect design. Jung et al. [12] showed that eccentric spear positioning in the nozzle (which is the case, when the axes of spear and nozzle are not coincident) leads to large water jet deformations and penalises therefore the efficiency. The numerical results have been compared qualitatively to experimental observations. Santolin et al. [4] compared the numerical results for an ideal jet and a real jet driving the runner and could show the reduction of runner efficiency due to the presence of secondary flows in the real jet. The final part of the penstock was included in the simulation domain, which adversely affected the Pelton turbine efficiency. Although real-life conditions can be investigated by numerical simulations, the flow predictions in the distributor line are often performed with over-simplified assumptions for the inflow boundary conditions.

Through numerical simulation of a typical Pelton turbine manifold scenario, we show how the generation of losses and secondary flows in the distributor line is affected by different inflow modelling assumptions. First, several turbulence models are tested to investigate their influence on the flow in the distributor. Further, we explore the sensitivity of the flow predictions to variations of the inflow turbulence intensity. The distributor "quality" is evaluated by different criteria, including the pressure drop, the entropy generation, the ratio of secondary flow velocity to primary flow velocity, and the distribution of mass flow inside the injectors. Thereby, we demonstrate how the modelling of the upstream flow history affects the distributor quality, which should not be neglected in the design and optimisation of distributor lines.

2. Introduction of quality criteria for distributor pipes

2.1. Head loss coefficient from decrease of total pressure

Similarly to Dixon and Hall's [13] definitions of total pressure loss coefficients for turbomachinery cascades, we introduce the head loss coefficient as the decrease of total pressure between two designated stations of the distributor

$$K_{pt} = \frac{p_{t,0} - p_{t,j}}{\rho u_0^2/2} \tag{1}$$

where $p_{t,j}$ is the total pressure, $p_{t,j} = p_j + \rho u_j^2/2$ evaluated at an arbitrary station j and u_0 is the mass flow-averaged velocity at the reference station 0 (see also figure 1). The head loss coefficient, as defined in equation (1), is only valid for pipes without branches. For the correct application of this principle to the distributor, we define an overall head loss coefficient for the entire distributor by weighing the individual contributions of every injector by their mass flow rate,

$$K_{pt,USI} = \frac{p_{t,0} - \sum_{i=1}^{n} \frac{\dot{m}_i}{\dot{m}} \cdot p_{tUSI,i}}{\rho u_0^2/2} \ . \tag{2}$$

Equation (2) is exemplarily evaluated between the reference station 0 and the last stations of every branch upstream of the injector (USI).

2.2. Head loss coefficient from local entropy generation

Alternatively to equation (2) we compared the applicability of the Second Law Analysis (SLA) method introduced by Herwig and Schmandt [14] as a non-traditional way to assess the head loss coefficient in the distributor pipe. Based on the second law of thermodynamics, Herwig and Schmandt [14] define the loss coefficient by means of the non-reversible entropy generation rate $\dot{S}_{irr,D}$

$$K_\varphi = \frac{2 \cdot T_m \cdot \dot{S}_{irr,D}}{\dot{m} \cdot \rho \cdot u^2} \ . \tag{3}$$

By using the local volumetric dissipation rate Φ''' which is linked to the non-reversible local entropy generation rate $\dot{S}'''_{irr,D}$ by the mean thermodynamic temperature T_m

$$\Phi''' = T_m \cdot \dot{S}'''_{irr,D} = 2\mu \left\{ \left(\frac{\partial u_i}{\partial x_i} \right)^2 + \frac{1}{2} \left[\left(\frac{\partial u_i}{\partial x_j} + \frac{\partial u_j}{\partial x_i} \right)^2 \right] \right\} \tag{4}$$

and integrating over the control volume V_{IM}, which ranges from station 0 to the stations in the mid of the six injectors (IM) the definition of K can be expanded to

$$K_{\varphi,IM} = \frac{2T_m}{\dot{m} u_m^2} \int_{V_{IM}} \dot{S}''' \mathrm{d}V = \frac{2}{\dot{m} u_m^2} \int_{V_{IM}} \dot{\Phi}''' \mathrm{d}V \ . \tag{5}$$

With Reynolds-averaging, the dissipation Φ''' is split into a time averaged part $\overline{\left(\dot{\Phi}'''\right)}$, also called viscous dissipation $\dot{\Phi}'''_v$ and a fluctuating part $\left(\dot{\Phi}'''\right)'$, also called turbulent dissipation $\dot{\Phi}'''_t$, i.e. $\Phi''' = \overline{\left(\dot{\Phi}'''\right)} + \left(\dot{\Phi}'''\right)'$. Analogously, the head loss coefficient can be divided into two parts, $K_{\varphi v,IM}$ and $K_{\varphi t,IM}$. The time-averaged part of the dissipation can be computed by applying the time-averaged flow velocity $\overline{\vec{u}} = (\overline{u}, \overline{v}, \overline{w})$ to equation (4). Schmandt and Herwig [15] proposed to model the turbulent dissipation as

$$\dot{\Phi}'''_t = \left(\dot{\Phi}'''\right)' = \rho\varepsilon = \beta^* \rho\omega k \ . \tag{6}$$

This relationship implies that the estimation of the entropy production, and hence, the head loss coefficient rely on the selected turbulence closure model used to compute the turbulent eddy frequency ω and the turbulent kinetic energy k.

2.3. Quantification of secondary flows

The flow velocity $\vec{u} = (u, v, w)$ can be split into a primary component in principal flow direction (I) and a secondary component (II) perpendicular to the principal flow direction, i.e. $\vec{u} = \vec{u}_I + \vec{u}_{II}$. The principal flow direction is defined as the streamwise coordinate $\vec{s}$ along the centerline of the distributor line, and thus, $\vec{u}_I = \vec{u} \cdot \vec{s}$ and $\vec{u}_{II} = \vec{u} - \vec{u} \cdot \vec{s}$. The ratio of the secondary to the principal velocity magnitude can be defined for an arbitrary station, j, as $\phi_{II,j} = (u_{II}/u_I)_j$. A secondary velocity ratio can be defined as the velocity components weighted by the corresponding mass flow rate summed over all injectors;

$$\phi_{II,USI} = \frac{\sum_{i=1}^{n} \dot{m}_{USI,i} \cdot u_{II,USI,i}}{\sum_{i=1}^{n} \dot{m}_{USI,i} \cdot u_{I,USI,i}} \ . \tag{7}$$

2.4. Criterion for mass flow imbalances

The water jet impulse shall be distributed equally to the Pelton turbine runner for smooth operation. Circumferential imbalances of the mass flow rates at the nozzle crucially affect the water jet formation. The sum-square error between the left and the right sides of the flow path in the six injectors,

$$\varepsilon_{IM} = \sqrt{\sum_{i=1}^{n} \left(2 \cdot \frac{\dot{m}_{l,i} - \dot{m}_{r,i}}{\dot{m}_i} \right)^2} , \tag{8}$$

indicates the non-uniformity imposed by the upstream pipe bends. The indices l and r denote the left and the right side of the flow path in direction towards the nozzle exit.

3. Numerical methodology

The investigated distributor geometry with six injectors (I1 to I6) is shown in figure 1. A water mass flow rate corresponding to a Reynolds number of $Re_0 = Re(D_0) = 9 \cdot 10^5$ is set for all cases together with the zero pressure gradient as the inflow boundary condition. The velocity profile at the inlet is extrapolated from the next cell in the domain. The static pressure is set to standard atmospheric conditions with a zero velocity gradient boundary condition at all outlets. If not stated otherwise, a turbulence intensity of 5% together with the hydraulic diameter was prescribed for the turbulence quantities at the inlet section of all cases. The properties for water were the density, $\rho_{water} = 1000\ kg/m^3$, and the kinematic viscosity, $\nu_{water} = 1 \cdot 10^{-6}\ m^2/s$, and for air were the density, $\rho_{air} = 1\ kg/m^3$, and the kinematic viscosity, $\nu_{air} = 1.48 \cdot 10^{-5}\ m^2/s$. The surface tension coefficient between water and air is $\sigma = 0.07\ N/m$.

All simulations were performed with the open-source CFD software OpenFOAM v2012. The multi-phase solver *interFoam*, based on the Volume-of-Fluid (VOF) approach with interface capturing [16], was employed to capture the nature of the incompressible and isothermal flow of the two immiscible fluids. Turbulence was modelled by considering the Reynolds averaged Navier-Stokes equations (RANS). A local time-stepping approach was employed for time discretisation, where the cell-based pseudo-time-step was limited to a Courant number of 0.5. The gradients were computed using a cell-limited least-squares scheme. The convection terms were solved using a first-order upwind scheme, and a van Leer limited scheme advected the water/air interface.

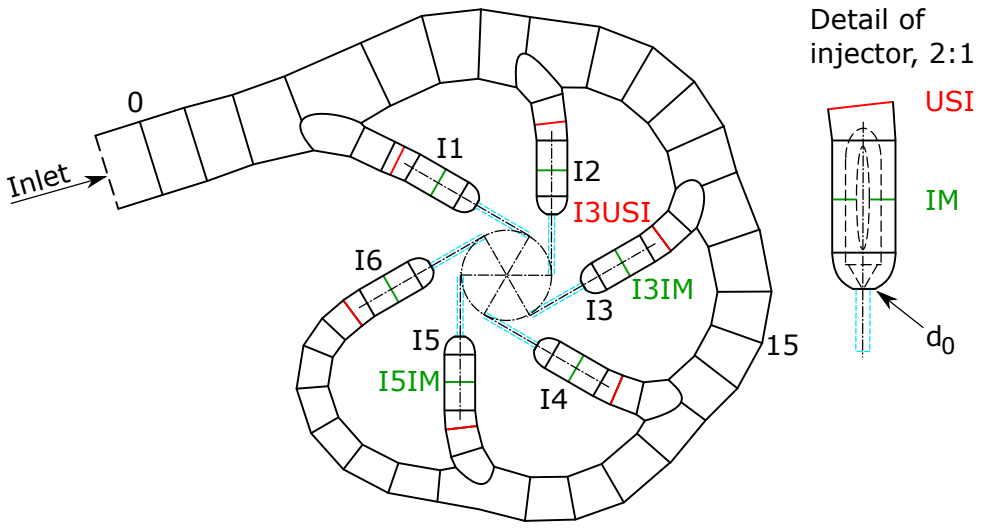

Figure 1. Geometry of the investigated distributor line. Red lines indicate the stations upstream the injectors (USI), the green lines indicate the stations in the mid of the injectors (IM).

Table 1. Discretisation errors of the quality criteria.

	$K_{pt,IM}$	$K_{\varphi,IM}$	$\varphi_{II,USI}$	$\varepsilon_{Injectors}$
N_1, N_2, N_3		$(20.0, 7.4, 4.0) \cdot 10^6$		
r_{21}, r_{32}		1.395, 1.233		
ϕ_1	0.553	0.326	0.070	0.127
ϕ_2	0.595	0.314	0.066	0.135
ϕ_3	0.742	0.208	0.063	0.133
p	6.71	10.80	0.77	3.13
ϕ_{ext}^{21}	0.548	0.326	0.084	0.123
e_a^{21}	7.7%	3.7%	5.5%	6.4%
e_{ext}^{21}	0.9%	0.1%	15.8%	3.6%
GCI_{fine}^{21}	1.2%	0.1%	23.5%	4.38%

A grid resolution study was performed following the methodology proposed by Celik et al. [17], where the $k-\omega$ SST turbulence model was employed. The three block-structured meshes had $4.0 \cdot 10^6$, $7.4 \cdot 10^6$, and $20.0 \cdot 10^6$ hexahedral cells. The average y^+ value at the walls was 1.2 and was held constant for all grids. The numerical uncertainties of the integral quantities are listed in table 1. Both head loss coefficients $K_{pt,IM}$ and $K_{\varphi,IM}$ show excellent convergence with a grid convergence index of 1.2% and 0.1%, respectively. The secondary flow reacts sensitive to grid refinements, thus yielding a higher grid convergence index of 23.5%. The mass flow distribution criterion inside the injectors $\varepsilon_{Injectors}$ has an error of less than 5%.

The grid convergence errors for velocity magnitude profiles at stations I3 USI and 15 were evaluated to judge for an adequate mesh resolution.

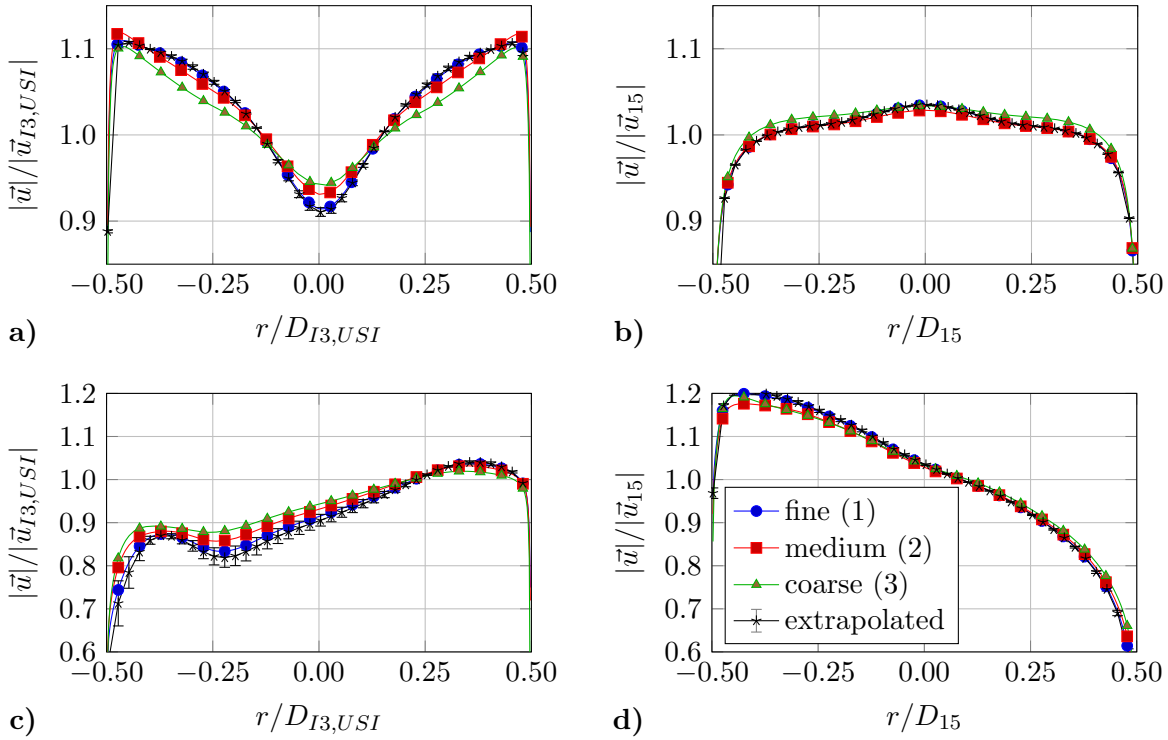

Figure 2. Velocity magnitude profiles normalised by the mass-flow averaged velocity magnitude for fine, medium, and coarse grid including the extrapolated velocity profiles with error bars: a) Profiles along a vertical line in station I3 USI, b) Profiles along a vertical line in station 15, c) Profiles along a horizontal line in station I3 USI, d) Profiles along a horizontal line in station 15.

Figure 2 shows that with grid refinement, the velocity profiles converge towards the extrapolated value. The global average of the order of accuracy p_{ave} lies between 3 for the velocity profiles at station I3 USI and 4.9 for the velocity profiles at station 15, where 30% and 41% of the points show oscillatory convergence, respectively. The local maximum discretisation uncertainty GCI_{max} is below 3.9% at station 15 and 5.3% at station I3 USI. The medium mesh was chosen for subsequent simulations, providing the best balance between computational effort and result accuracy.

4. Results

4.1. Influence of turbulence model

Turbulence modeling impacts the prediction of flow losses and secondary flows in Pelton turbine distributors. Five different Reynolds-average Navier-Stokes (RANS) turbulence closures were employed to investigate the sensitivity of the performance evaluation on the turbulence model. The one equation model of Spalart and Allmaras (SA) [18], the Standard k-ε model (kE) of Launder and Spalding [19], the k-ω Shear Stress Transport model (SST) of Menter [20], the Standard k-ω model (kw) of Wilcox [21], and the three equation transition model k-kl-ω (k-kl-w) of Walters and Cokljat [22] were used.

The flow losses and the amount of secondary flows predicted with the considered turbulence models are compared in figure 3. The head loss coefficients have been computed based on the total pressure drop between station 0 and stations USI (equation (2)), and by applying the Second Law Analysis method (equation (5)). The amount of secondary flow in stations USI and IM is calculated by the means of equation (7). Head loss coefficients $K_{pt,USI}$ of about 0.55 are predicted with the kw, the SST model, and the SA model, whereas the kE and the k-kl-w model estimate significantly lower head losses. A possible explanation for this result can be found comparing the flow fields shown in figure 4, where the velocity magnitude contours are plotted in the symmetry plane of the distributor line. Below, the secondary flow velocity contours at the mid of injector 5 are depicted. Both sets of contour plots were normalised by the velocity magnitude at station 0. The symmetry plots reveal a much more even velocity distribution for the kE model case compared to those of the SA and the SST model. While the flow looks similar for the SA and SST model cases, the magnitudes at the inside of the distributor line are observably higher in the case of the SST model. This becomes particularly apparent for the

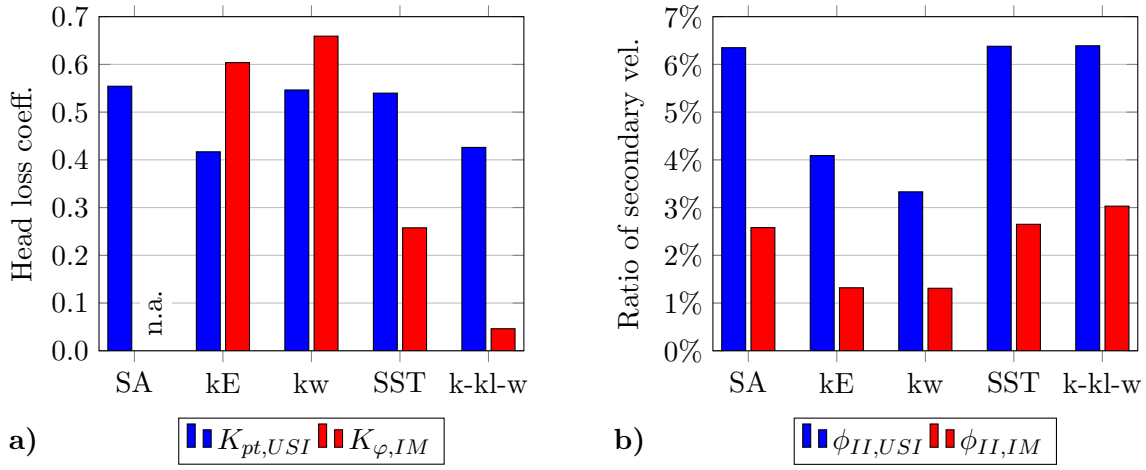

Figure 3. Head loss coefficients obtained using the total pressure loss and the entropy production (a) and secondary velocity ratios (b) for different turbulence models. Quantities are evaluated at stations upstream the injectors (USI) and at the mid of the injectors (IM).

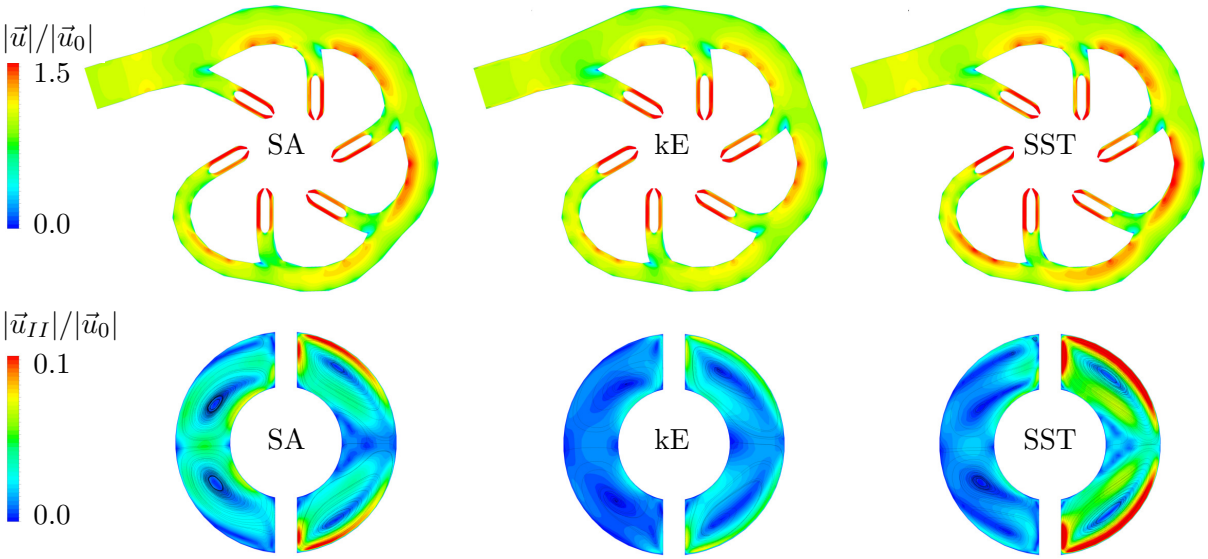

Figure 4. Velocity contour plots for three turbulence models. Upper row: Velocity magnitude in the symmetry plane of the distributor pipe. Lower row: Magnitude of the secondary velocity in a station in the mid of injector 5 (I5 IM). The view is oriented towards the downstream direction.

pipe sections upstream and downstream of injector 5 and is further emphasised by the strong and unevenly distributed secondary flow in station I5 IM for this model. The kE model features less secondary flow and a more even distribution. On that account, it seems the kE model as well as the k-kl-w model are under-predicting the head loss compared to the other models. Figure 3 also reveals the variation of head loss coefficients $K_{\varphi,IM}$ obtained. Obviously, the results depend on the boundary layer resolution and the near-wall formulation of the turbulence model. Thus, judging which turbulence model predicts the head loss from entropy generation correctly is challenging without additional information.

The secondary flow ratio is above 6% at the station USI and between 2.5% to 3.0% at the station IM with the SA, SST, and k-kl-w models. This reduction of secondary flows can be attributed to a throttling effect when the flow enters the annular space in the injectors. The kE and the kw models predict lower values for the secondary flow ratios at both stations. Two observations are noteworthy comparing the head losses and the secondary flow ratios predicted with the considered turbulence models. Selecting the most trustworthy turbulence model is impossible without experimental data. However, the SST model allowed for reasonably accurate computation of both head loss and secondary flows and was therefore used in all subsequent simulations. The SA model exhibits similar results as the SST model. Considering the computational efficiency, it is worthwhile considering the SA model, especially for rapid design and optimisation, where computational time is a limiting factor.

4.2. Variation of turbulence intensity at the inlet

In this subsection, we discuss the effect of varying inlet turbulence intensities TI_{Inlet} on the head loss, amount of secondary flow and mass flow rate distribution. While specifying an inlet turbulence intensity of 5% is a common engineering assumption for many internal flow problems in hydraulic machinery applications, we varied TI_{Inlet} from 1% (very low) to 10% (high) applying the SST turbulence model.

Figure 5 compares the head losses, secondary flow ratio, and the mass flow rate distribution against the turbulence intensity level at station 0. With increasing TI_0, both head loss curves, $K_{pt,USI}$ and $K_{\varphi,IM}$, follow an almost parallel upward trend from about $\mathrm{TI}_0 = 3\%$ upwards.

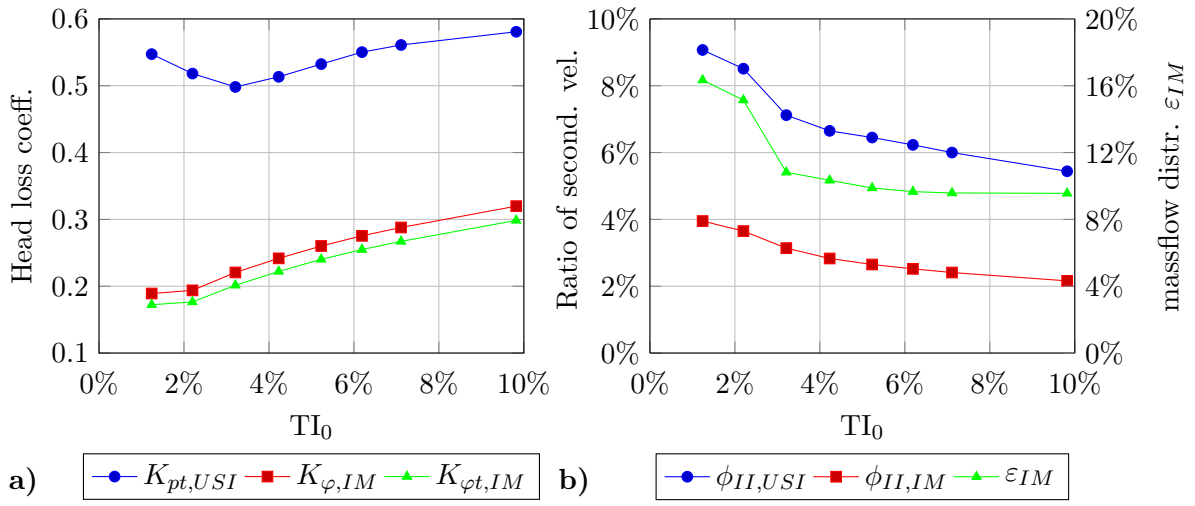

Figure 5. Variation of head loss coefficients obtained from the total pressure loss and from the entropy production (a) and the secondary velocity ratio and mass flow rate distribution (b) as a function of turbulence intensity TI_0 at station 0. Quantities are evaluated at stations upstream the injectors (USI) and in the mid of the injectors (IM).

Below $TI_0 = 3\%$, $K_{\varphi,IM}$ levels off and $K_{pt,USI}$ shows a gradual increase with declining turbulence intensity. The almost linear growth of $K_{\varphi,IM}$ can largely be attributed to an increase of turbulent dissipation $\dot{\Phi}_t'''$ (see equation (6)), while the viscous dissipation only rises slightly for turbulence intensities greater than 3%. This gain in $\dot{\Phi}_t'''$ correlates strongly to the increasing amount of turbulence in the domain for higher inlet turbulence levels and is highlighted in the contour plots of turbulent dissipation in figure 6. The turbulent dissipation constitutes about 90% and the viscous dissipation constitutes about 10% of the total dissipation between station 0 and station IM.

In contrast to the growth of head loss, the secondary velocity ratio decreases continuously with rising turbulence intensity levels at the stations upstream of the injectors (USI). After an initial drop-off below $TI_0 = 3\%$, a linear trend is observed. The contour plots shown in figure 6 show that the flow is not fully developed before reaching the first branch for the cases with low inlet turbulence. Therefore, the normalised velocity magnitude pattern in the symmetry plane looks entirely different from the pattern of the cases with higher turbulence intensities. A gradual reduction of secondary flows with increasing turbulence levels can be observed in the contour plots. Moreover, the general flow pattern does only change marginally from $TI_0 = 5\%$ to $TI_0 = 10\%$ compared to the differences observable between $TI_0 = 1\%$ and $TI_0 = 5\%$. This observation is emphasised by the contour plots of the secondary velocity in stations USI and IM of injector 3 as shown in the lower row of figure 6 and by the no longer declining mass flow rate distribution inside the injectors as plotted in figure 5 b). Therefore, choosing the right amount of inflow turbulence levels is critical for the accuracy of numerical predictions because the formation of secondary flows and turbulence kinetic energy is sensitive to small changes in the range of 1% to 4%. With typical installations to reduce turbulence in Pelton turbine manifolds, the practical turbulence levels are expected to occur in or slightly above this sensitive region.

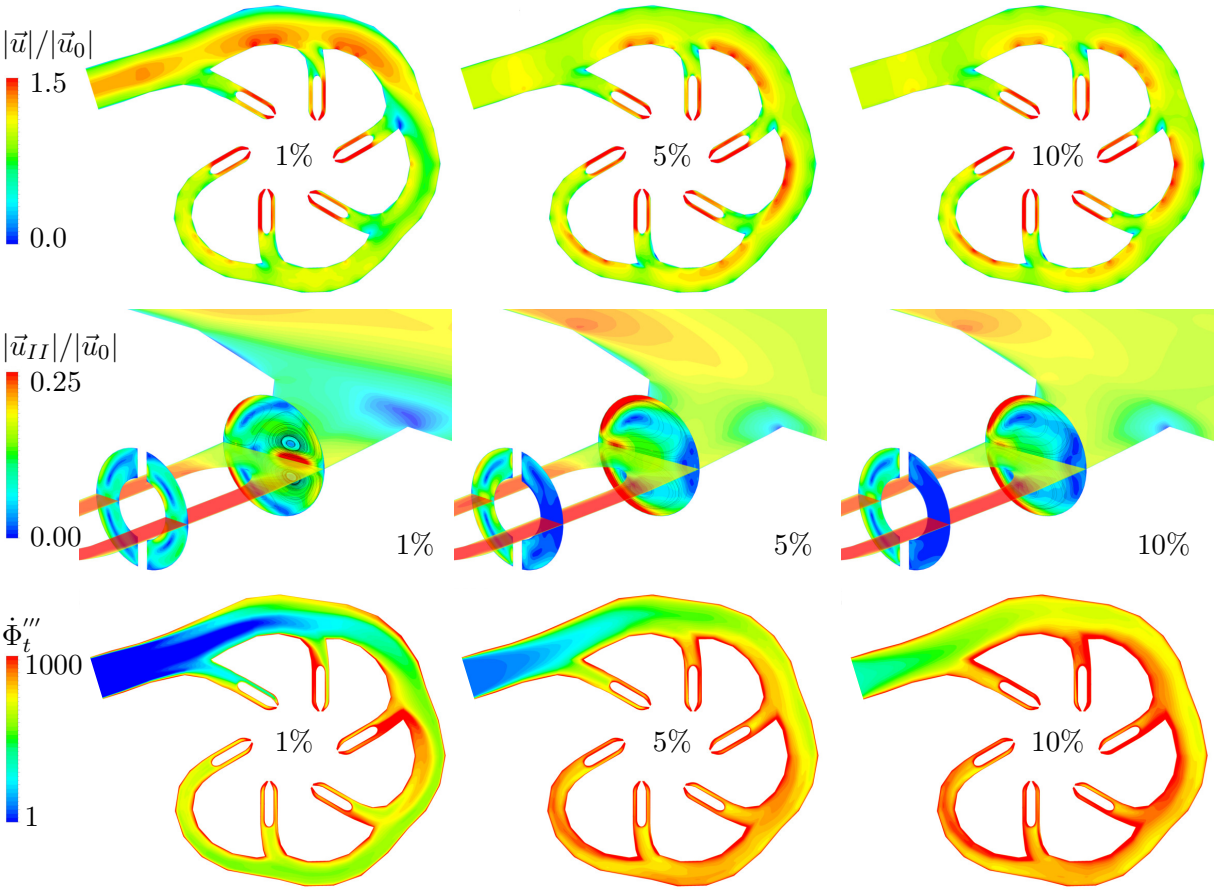

Figure 6. Contour plots for inlet turbulence intensities of 1%, 5% and 10%. Upper row: Velocity magnitude in the symmetry plane of the distributor pipe. Mid row: Magnitude of the secondary velocity in stations upstream (USI) and in the mid (IM) of injector 3 (and velocity magnitude in the symmetry plane). Lower row: Turbulent dissipation in the symmetry plane.

5. Conclusions

The present research was motivated by the widespread unchallenged use of over-simplified assumptions for the inflow boundary conditions when simulating the flow in Pelton turbine manifolds. We employed different criteria quantifying the flow quality in the distributor pipe and investigated how these criteria were affected by turbulence modelling and different inflow turbulence intensities. The findings of this paper underline that relying on over-simplified assumptions can lead to imprecise conclusions and wrong design alterations. Therefore, we recommend to carefully select appropriate inflow boundary conditions.

The test of five different turbulence models revealed drastic differences in the computed losses and secondary flow ratios that challenge selecting the most suitable model. Overall, the k-ω Shear Stress Transport model revealed reasonably accurate results. The computationally less expensive Spalart-Allmaras model exhibits a similar performance as the SST model and is, therefore, a good choice for optimisation problems. The variation of the inflow turbulence intensity showed that both criteria, the head losses and the secondary velocity ratio, keep changing with increasing inlet turbulence. Above a threshold of $\mathrm{TI}_{Inlet} = 4\%$, the flow patterns change only slightly, whereas the secondary flow increases significantly below this threshold. Since the flow reacts very sensitively to changes in the turbulence intensity below 4%, particular attention must be paid to the correct specification of the inflow properties, especially when

flow-calming or turbulence-reducing measures are in place.

A final remark has to be made on the Second Law Analysis method introduced in section 2.2. The head loss estimated by the SLA method was lower than the head loss based on the total pressure drop. An explanation for this may be the limited domain in which the dissipation was integrated. Herwig and Schmandt [23] emphasise the necessity of sufficiently long upstream and downstream integration domains, i.e. $15D_h$ and $25D_h$ for the case of a T-junction, when calculating the head loss from entropy production. Unfortunately, this requirement cannot be fulfilled for Pelton turbine distributor pipes given the tight packaging of the assembly. Thus, the application of the SLA method is not feasible for studying Pelton turbine manifolds losses.

Acknowledgments

The computational results presented have been achieved in part using the Vienna Scientific Cluster (VSC4). The authors acknowledge the financial support through the Österreichische Forschungsförderungsgesellschaft (FFG) under the projects 'AxFeeder' (project number 888084) and 'WakaSi' (project number 891635). The first author would like to thank the foundation of Christiana Hörbiger for sponsoring his participation at the symposium.

References

[1] Zhang Z and Casey M 2007 *Proc. Inst. Mech. Eng. A: J. Power Energy* **221** 1181–1192
[2] Staubli T, Abgottspon A, Weibel P, Bissel C, Parkinson E, Leduc J and Leboeuf F 2009 Jet quality and Pelton efficiency *Proceedings of HYDRO 2009 International Conference, Lyon, France*
[3] Peron M, Parkinson E, Geppert L and Staubli T 2008 Importance of jet quality on Pelton efficiency and cavitation *International Conference on Hydraulic Efficiency Measurements, Milan, Italy*
[4] Santolin A, Cavazzini G, Ardizzon G and Pavesi G 2009 *Proc. Inst. Mech. Eng. A: J. Power Energy* **223** 721–728
[5] Patel K, Patel B, Yadav M and Foggia T 2010 Development of Pelton turbine using numerical simulation *25th IAHR Symposium on Hydraulic Machinery and Systems, Timisoara, Romania*
[6] Mack R, Gola B, Smertnig M, Wittwer B and Meusburger P 2014 Modernization of vertical Pelton turbines with the help of CFD and model testing *IOP Conf. Ser.: Earth Environ. Sci.* vol 22 p 012002
[7] Jošt D, Škerlavaj A, Pirnat V, Morgut M and Nobile E 2019 Numerical prediction of efficiency and cavitation for a Pelton turbine *IOP Conf. Ser.: Earth Environ. Sci.* vol 240 p 062033
[8] Han L, Duan X, Gong R, Zhang G, Wang H and Wei X 2019 *Renew. Energy* **131** 159–167
[9] Xiao Y, Zeng C, Zhang J, Yan Z and Wang Z 2013 Numerical analysis of the bucket surface roughness effects in Pelton turbine *IOP Conf. Ser.: Mater. Sci. Eng.* vol 52 p 052032
[10] Chongji Z, Yexiang X, Wei X, Tao W, Jin Z, Zhengwei W and Yongyao L 2016 Numerical Analysis of Pelton Nozzle Jet Flow Behavior Considering Elbow Pipe *IOP Conf. Ser.: Earth Environ. Sci.* vol 49 p 022005
[11] Zeng C, Xiao Y, Luo Y, Zhang J, Wang Z, Fan H and Ahn S H 2018 *Renew. Energy* **125** 270–282
[12] Jung I H, Kim Y S, Shin D H, Chung J T and Shin Y 2019 *Energy* **175** 58–65
[13] Dixon S and Hall C 2010 *Fluid Mechanics and Thermodynamics of Turbomachinery (Sixth Edition)* (Butterworth-Heinemann) ISBN 978-1-85617-793-1
[14] Schmandt B and Herwig H 2011 *J. Fluids Eng.* **133** 051201
[15] Schmandt B and Herwig H 2011 *Entropy* **13** 1380–1402
[16] OpenCFD Limited *OpenFOAM v2012 User Guide* URL `https://www.openfoam.com/documentation/user-guide`
[17] Celik I B, Ghia U, Roache P J and Freitas C J 2008 *J. Fluids Eng.* **130** 078001
[18] Spalart P and Allmaras S 1992 A one-equation turbulence model for aerodynamic flows *30th Aerospace Sciences Meeting and Exhibit, Reno, NV, USA*
[19] Launder B and Spalding D 1974 *Comput. Methods Appl. Mech. Eng.* **3** 269–289
[20] Menter F R 1994 *AIAA J.* **32:8** 1598–1605
[21] Wilcox D 1994 *Turbulence Modeling for CFD* (DCW Industries, Incorporated) ISBN 9780963605108
[22] Walters D K and Cokljat D 2008 *J. Fluids Eng.* **130** 121401
[23] Herwig H and Schmandt B 2014 *Entropy* **16** 2959–2989